

## Continuum percolation of congruent overlapping polyhedral particles: Finite-size-scaling analysis and renormalization-group method

Wenxiang Xu,<sup>1,2,\*</sup> Zhigang Zhu,<sup>1</sup> Yaqing Jiang,<sup>1</sup> and Yang Jiao<sup>2,†</sup>

<sup>1</sup>College of Mechanics and Materials, Hohai University, Nanjing 211100, People's Republic of China

<sup>2</sup>Materials Science and Engineering, Arizona State University, Tempe, Arizona 85287, USA



(Received 7 June 2018; revised manuscript received 7 November 2018; published 6 March 2019)

The continuum percolation of randomly orientated overlapping polyhedral particles, including tetrahedron, cube, octahedron, dodecahedron, and icosahedron, was analyzed by Monte Carlo simulations. Two numerical strategies, (1) a Monte Carlo finite-size-scaling analysis and (2) a real-space Monte Carlo renormalization-group method, were, respectively, presented in order to determine the percolation threshold (e.g., the critical volume fraction  $\phi_c$  or the critical reduced number density  $\eta_c$ ), percolation transition width  $\Delta$ , and correlation-length exponent  $\nu$  of the polyhedral particles. The results showed that  $\phi_c$  (or  $\eta_c$ ) and  $\Delta$  increase in the following order: tetrahedron < cube < octahedron < dodecahedron < icosahedron. In other words, both the percolation threshold and percolation transition width increase with the number of faces of the polyhedral particles as the shape becomes more “spherical.” We obtained the statistical values of  $\nu$  for the five polyhedral shapes and analyzed possible errors resulting in the present numerical values  $\nu$  deviated from the universal value of  $\nu = 0.88$  reported in literature. To validate the simulations, the corresponding excluded-volume bounds on the percolation threshold were obtained and compared with the numerical results. This paper has practical applications in predicting effective transport and mechanical properties of porous media and composites.

DOI: [10.1103/PhysRevE.99.032107](https://doi.org/10.1103/PhysRevE.99.032107)

### I. INTRODUCTION

The continuum percolation of overlapping nonspherical particles has broad applications in geophysics and engineering. Examples include the rheology and transport processes in porous media, permeability and water saturation in hydrocarbon exploration, rock physics and fractures, and determination of thermal and electrical conductive, diffusive, dielectric, and elastic properties of granular materials [1–5], to name but a few. Specifically, the physical properties (e.g., diffusivity, permeability, conductivity, and elastic moduli) of a material can change dramatically as the percolation threshold (i.e., the critical volume fraction or reduced number density at which a system-spanning cluster or connected network of the objects of interest first emerges) is approached [5–11]. It is thus crucial to accurately determine the percolation threshold, as well as other important percolation properties such as the associated percolation transition width and the correlation-length exponent. Several studies on the continuum percolation of three-dimensional (3D) particle systems have been carried out, including permeable and/or impenetrable spheres [12–14], regular polyhedral particles [15], ellipsoids [16,17], spherocylinders [18–23], plates [24,25], superballs [10], and superellipsoids [26].

Despite the aforementioned important works in the area, accurate results on percolation characteristics are missing for a special class of the particle geometry, i.e., 3D polyhedra. Polyhedral shapes have been extensively studied in the context

of particle packing and self-assembly [27–29]. These shapes are also more realistic models for grains and pores in geomaterials [9], compared to the commonly employed models such as perfect spherical, ellipsoidal, or spherocylindrical shapes. How the unique geometric features of polyhedral particles (e.g., sharp edges, corners, and flat facets) affect the percolation properties (especially the percolation threshold) remains elusive. The percolation thresholds of overlapping cubes and octahedra have received some attention recently, including theoretical approximations based on the excluded-volume theory [10,15,30] and numerical simulations [9,15,31]. In addition, the numerical values of the percolation threshold characterized by the critical reduced number density  $\eta_c$  for randomly oriented overlapping Platonic solids including tetrahedron, octahedron, cube, dodecahedron, and icosahedron have been estimated in Ref. [15]. Specifically, the authors employed a highly efficient rescaled particle method to obtain the percolation threshold for a given shape for various system sizes, and extrapolated the estimates to infinite-sized systems. However, it is still challenging to quantitatively understand the continuum percolation of polyhedral particles, especially to accurately determine the percolation threshold, percolation transition width, and correlation-length exponent for these shapes.

In this paper, we present two numerical frameworks—the Monte Carlo finite-size-scaling (MCFSS) analysis and the real-space Monte Carlo renormalization-group (MCRG) method—to, respectively, investigate the continuum percolation of randomly oriented congruent overlapping polyhedral particles, including tetrahedron, cube, octahedron, dodecahedron, and icosahedron under periodic boundary conditions, following Refs. [15,32]. It has been shown that the MCFSS

\*xwxfat@gmail.com

†yang.jiao.2@asu.edu

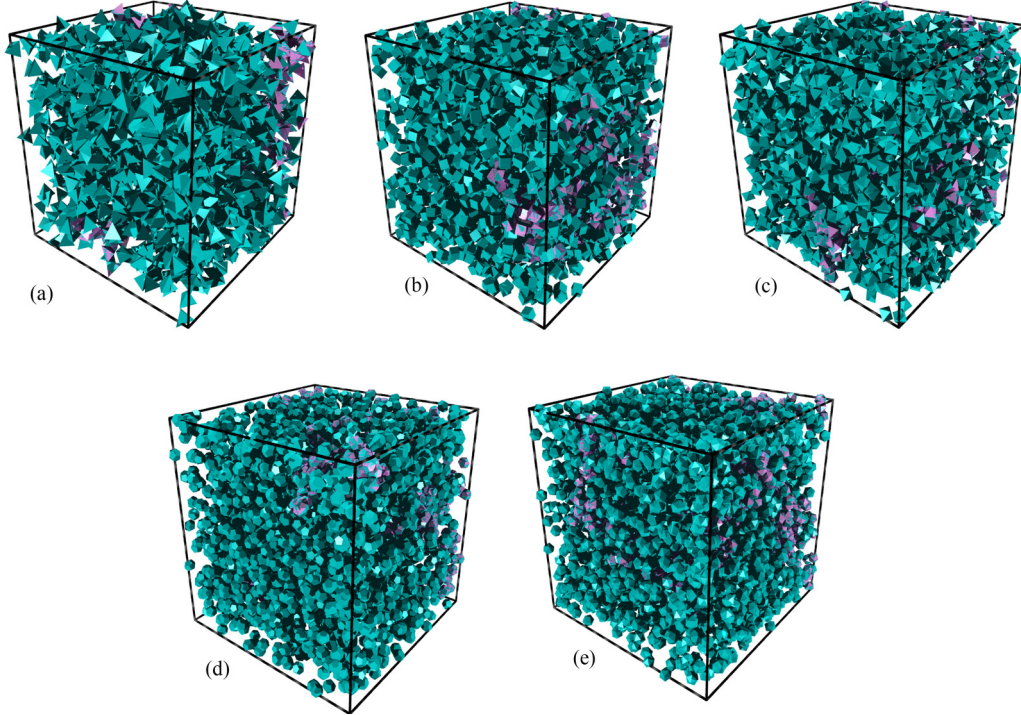


FIG. 1. Visualizations of random dispersions of overlapping polyhedral particles of  $R_{\text{eq}} = 1.0$ , including (a) tetrahedron, (b) cube, (c) octahedron, (d) dodecahedron, and (e) icosahedron. The orchid particles in each box belong to a percolating cluster under periodic boundary conditions (see Fig. 2).

analysis and the MCRG method are effective strategies for the accurate determination of percolation threshold in the infinite-system limit [1–3]. The percolation probability  $P$ , percolation transition width  $\Delta$ , and correlation-length exponent  $\nu$ , in addition to the percolation threshold represented by the critical volume fraction  $\phi_c$  and the critical reduced number density  $\eta_c$ , are obtained. In addition, the excluded-volume bounds on percolation threshold are computed to ascertain the accuracy of the present numerical results.

The rest of the paper is organized as follows. In Sec. II, we provide details of the Monte Carlo simulations for identifying the percolating clusters and the percolation probability. In Sec. III, we present the MCFSS scheme to derive the percolation transition width, the correlation-length exponent  $\nu$ , and the percolation threshold for the five polyhedral shapes. In addition, we describe the MCRG method to obtain  $\nu$  and  $\phi_c$  for the five polyhedral shapes. The excluded-volume percolation bounds are also computed. Finally, our conclusions and remarks are presented in Sec. IV.

## II. METHODS

The system of interest is a two-phase mixture consisting of randomly oriented congruent overlapping polyhedral particles randomly placed in a homogeneous matrix with periodic boundary conditions (Fig. 1). We note that both the positions and orientations of the particles are totally uncorrelated and follow the Poisson distribution. Size polydispersity of the particles does not appear to significantly influence the percolation threshold in an infinite system [1,3,20–22] and, thus, is not considered here.

For convenience, we use a cubic simulation box of size  $L$  for each realization of the system. For continuum percolation models, the percolation probability  $P(\phi, L)$  should be first probed. Here, we define  $P$  as the ratio of the number of percolated realizations to the total number of realizations for a given particle volume fraction  $\phi$  and a system size  $L$ . To accurately determine  $P(\phi, L)$ , we generate a large number of independent realizations, in which the number  $N$  of overlapping particles in a cubic realization is calculated by

$$N = \frac{-L^3}{V} \ln(1 - \phi) \quad (1)$$

where  $V$  is the volume of a polyhedron. We adopt the equivalent radius  $R_{\text{eq}}$  to characterize the linear size of a polyhedron, which is defined as the radius of an equivalent sphere having the same volume as the polyhedron [33]. It is a robust size descriptor for a complex nonspherical particle with respect to both the side length and the number of faces of a polyhedron reported in the literature. Accordingly, for an arbitrary polyhedral particle, its volume can be written as  $V = 4\pi R_{\text{eq}}^3/3$ . Specifically, the side length  $l$  of a polyhedron is related to  $R_{\text{eq}}$  by  $R_{\text{eq}} = l/2b$ , where  $b = (\sqrt{2}/2\pi)^{-1/3}$  for the tetrahedron,  $b = (6/\pi)^{-1/3}$  for the cube,  $b = (2\sqrt{2}/\pi)^{-1/3}$  for the octahedron,  $b = [(45 + 21\sqrt{5})/2\pi]^{-1/3}$  for the dodecahedron, and  $b = [(15 + 5\sqrt{5})/2\pi]^{-1/3}$  for the icosahedron [34].

In order to check the connected pathway (i.e., the emergence of the percolating cluster) in each realization, it is critical to detect the overlap between a pair of adjacent particles. For polyhedral particles, we adopt the separation axis scheme [27] to detect possible overlap between two polyhedra.

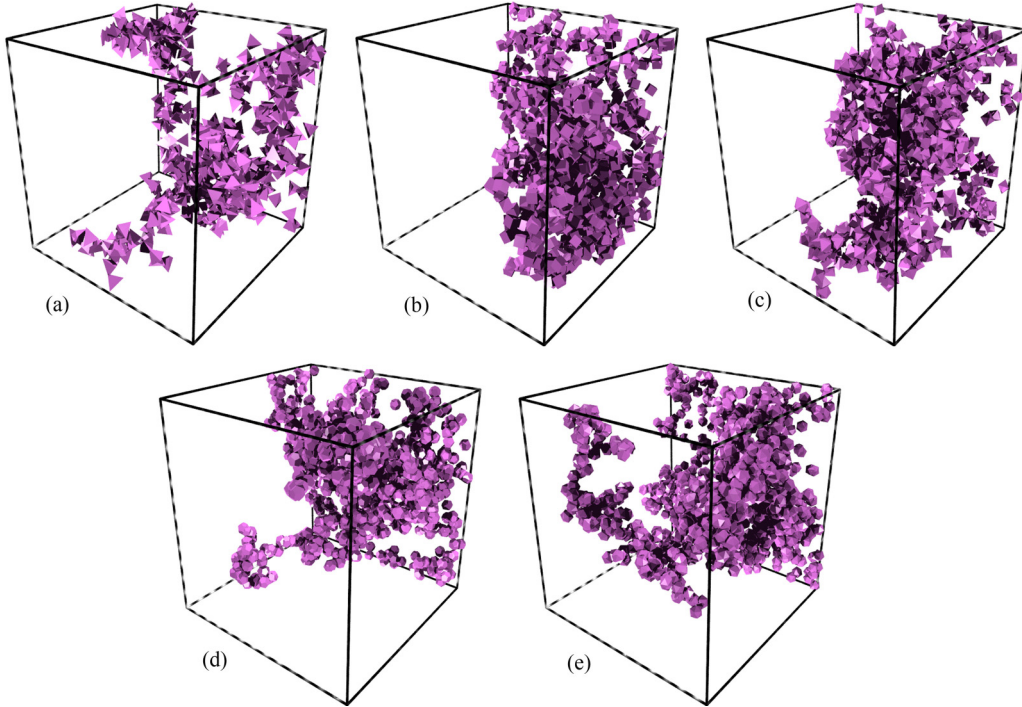


FIG. 2. Visualizations of the percolating cluster in the corresponding representative realizations for each shape shown in Fig. 1.

Specifically, if there is an axis onto which the intervals of projections of two polyhedra do not intersect, the two polyhedra do not overlap; otherwise, they overlap. In addition, a geometrical algorithm for detecting the intersection between a polyhedron and a boundary plane has been described in the literature [34]. Then, a “tree-burning” algorithm [22] is utilized to search the connected pathway in each realization. Note that the “wrapping criterion” [12,35] is invoked in our simulations for determining the connected pathway under periodic boundary conditions. In this paper, we consider the system is percolated if a connected path along any of the three directions is formed. Figure 2 shows the percolating clusters (from the top plane to the corresponding bottom plane) in representative realizations for the five polyhedral shapes. The percolation probability  $P(\phi, L)$  can be subsequently determined for given  $\phi$  and  $L$ .

Figure 3 presents the percolation probabilities  $P(\phi, L)$  with different  $\phi$  and  $L$  for the five polyhedral shapes. It can be seen from Fig. 3 that  $P$  increases with  $\phi$ , and the  $P$ - $\phi$  curves shift to lower volume fractions, with unchanged shape, for different polyhedral particles. Nevertheless, the position of the  $P$ - $\phi$  curve is determined primarily by the shape of polyhedra, as shown in Fig. 4(a). On the other hand, the curves for different shapes collapse on a single universal curve when rescaled with  $[\phi - \phi_c(L)]/\Delta(L)$ , as shown in Fig. 4(b), where the definitions of  $\phi_c(L)$  and  $\Delta(L)$  are introduced in the following section.

### III. RESULTS

#### A. MCFSS analysis

As mentioned above, the critical volume fraction of polyhedral particles, at which a system-spanning cluster crossing any of the three dimensions emerges, is used as the percolation threshold for the system, since it can be directly applied to

predict the effective physical properties of porous and cracked media [8–10,23]. It is worth mentioning that the critical volume fraction has two forms—the local critical volume fraction [the local percolation threshold,  $\phi_c(L)$ ] and the global critical volume fraction (the global percolation threshold,  $\phi_c$ ), respectively, corresponding to finite-size systems and infinite-size systems. For the local percolation threshold, it is straightforward to measure  $\phi_c(L)$  in a finite-size system via the Monte Carlo simulations. However, the derivation of the global percolation threshold for an infinite-size system is more challenging in practice. According to the finite-size-scaling theory in lattice percolation [3,36],  $\phi_c$  is related to the local critical volume fraction  $\phi_c(L)$  via

$$\Delta(L) \propto L^{-1/\nu}, \quad \phi_c(L) - \phi_c \propto L^{-1/\nu} \quad (2)$$

where  $\Delta(L)$  characterizes the percolation transition width, which has not been systematically investigated in the continuum percolation of polyhedral particles. The quantity  $\Delta(L)$  indicates that for systems of finite size  $L$  the transition from nonpercolated to percolated states (and vice versa) as measured by the percolation probability  $P$  is associated with a width [3,12,37,38].  $\nu$  is the correlation-length exponent. As can be seen in Eq. (2), it is a prerequisite to obtain  $\Delta(L)$ ,  $\nu$ , and  $\phi_c(L)$ , in order to accurately determine the global percolation threshold using the scaling scheme. We employ Eq. (3) [12] to fit each curve of  $P$ - $\phi$  that follows the sigmoidal shape. Note that Eq. (3) is an approximation rather than an analytical formalism:

$$P(\phi, L) = \frac{1}{2} \left[ 1 + \tanh \left( \frac{\phi - \phi_c(L)}{\Delta(L)} \right) \right]. \quad (3)$$

Consequently, the local percolation threshold  $\phi_c(L)$  and percolation transition width  $\Delta(L)$  for each finite system size  $L$  can be statistically derived. To ensure the reliability of

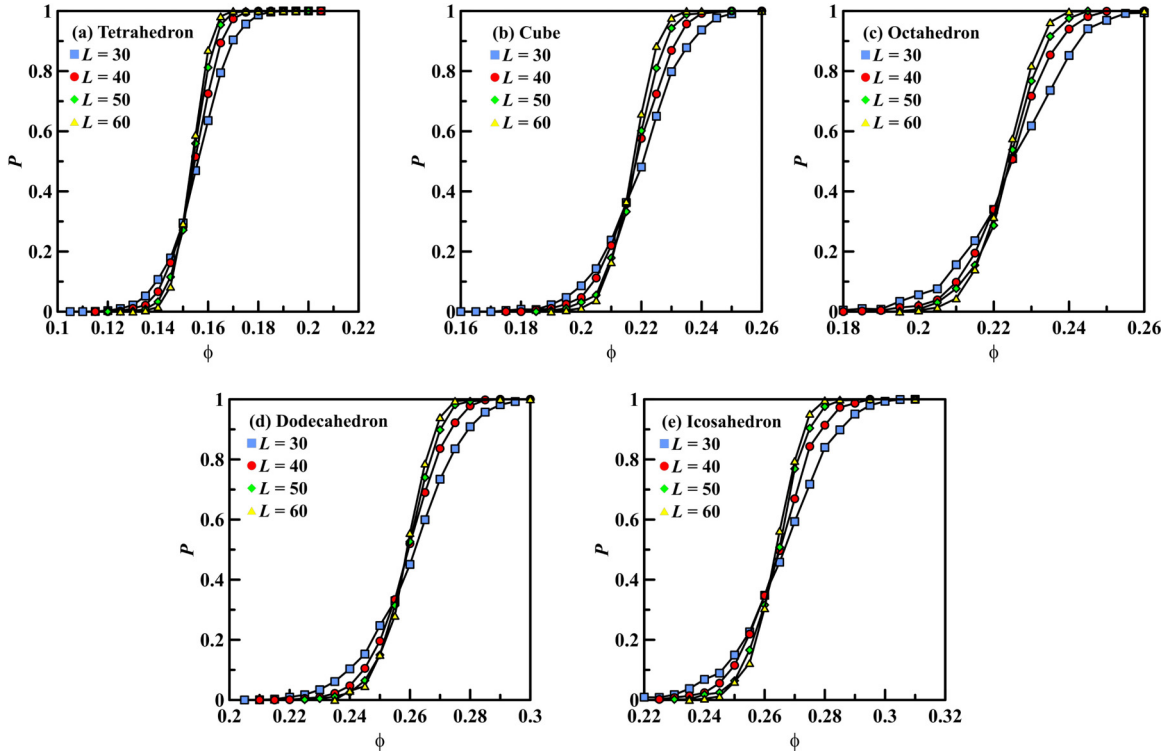


FIG. 3. The  $P$ - $\phi$  curves of various system sizes  $L$  for different polyhedral shapes: (a) tetrahedron, (b) cube, (c) octahedron, (d) dodecahedron, and (e) icosahedron. The symbols are the numerical results obtained using ensemble averaging whereas the solid lines are fittings based on Eq. (3).

statistical results, the size and number of realizations should be large enough. Accordingly, in our simulations,  $L = 30, 35, 40, 45, 50, 55,$  and  $60$ , and  $R_{eq} = 1$ , though the  $P$ - $\phi$  curves for  $L = 30, 40, 50,$  and  $60$  are only plotted in Fig. 3. Also, the number of realizations is assigned to be 15 000.

Figure 5 shows that the transition width  $\Delta$  for the five shapes monotonically decreases with increasing  $L$ . For a constant  $L$ ,  $\Delta$  increases in the following order: tetrahedron < cube < octahedron < dodecahedron < icosahedron. In other words,  $\Delta$  increases with increasing number of polyhedral faces, as shown in Fig. 5(a). According to the scaling relation in Eq. (2), in order to further obtain the correlation-length exponent  $\nu$ , we need to transform the numerical data depicted in Fig. 5(a) to the logarithmic values, since the linear slope of a plot of  $\ln(\Delta)$  versus  $\ln(L)$  corresponds to  $-1/\nu$ , as shown in Fig. 5(b).

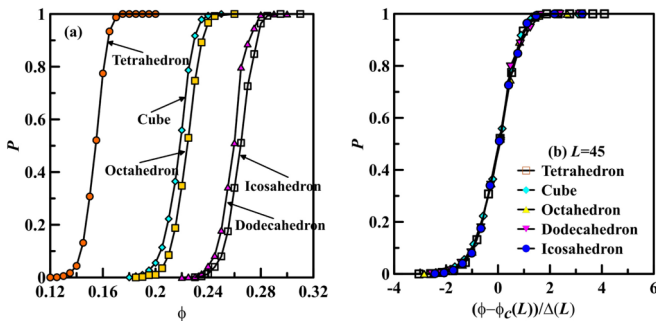


FIG. 4. The  $P$ - $\phi$  curves for  $L = 45$  for the five shapes of polyhedral particles shown as (a) separate curves and (b) collapsed on a universal curve when rescaled with  $[\phi - \phi_c(L)]/\Delta(L)$ .

Table I displays  $\nu$  for the five polyhedral shapes using the present MCFSS analysis.

After deriving  $\nu$  and  $\phi_c(L)$ , the global percolation threshold  $\phi_c$  is subsequently estimated from the scaling relation in Eq. (2). We present the numerical results of  $\phi_c(L)$  versus  $L^{-1/\nu}$  for the five polyhedral shapes and linearly fit these data to determine  $\phi_c$  that corresponds to the interception value of each  $\phi_c(L) - L^{-1/\nu}$  curve with the  $y$  axis, as shown in Fig. 6. To test the accuracy of the MCFSS analysis, we utilize the same scheme to derive  $\phi_c$  of the simplest interpenetrating sphere system and obtain  $\phi_c = 0.2896$ . This result is in excellent agreement with the numerical results reported by Rintoul and Torquato ( $\phi_c = 0.2895$ ) [12] and Lorenz and Ziff ( $\phi_c = 0.289573$ ) [39]. Both results are acknowledged as the most precise statistical values for  $\phi_c$  of the interpenetrating sphere

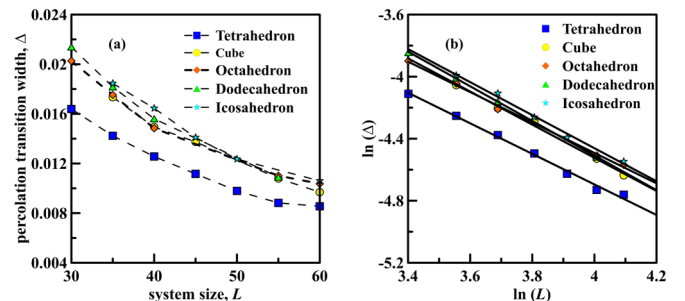


FIG. 5. Percolation transition width  $\Delta$  vs system size of  $L$  for different polyhedral shapes.

TABLE I. The correlation-length exponent  $\nu$  for the five polyhedral shapes from MCFSS analysis and MCRG method.

$\nu$	Tetrahedron	Cube	Octahedron	Dodecahedron	Icosahedron
MCFSS	$1.015 \pm 0.020$	$0.936 \pm 0.014$	$1.019 \pm 0.016$	$0.896 \pm 0.015$	$0.939 \pm 0.015$
MCRG ( $L_0 = 8$ )	$1.017 \pm 0.018$	$0.937 \pm 0.012$	$1.016 \pm 0.015$	$0.892 \pm 0.013$	$0.939 \pm 0.015$
MCRG ( $L_0 = 9$ )	$1.015 \pm 0.017$	$0.942 \pm 0.012$			

system obtained to date. In addition, our result of  $\phi_c = 0.2151$  for cubic particles is consistent with the numerical result of  $\phi_c = 0.2168$  reported by Baker *et al.* [31], and with the Padé approximation of  $\phi_c = 0.2106$  from Alon *et al.* [30]. These comparisons strongly indicate the accuracy of the present numerical framework for the determination of the global percolation threshold  $\phi_c$  of polyhedral particles. The statistical results of  $\phi_c$  for the five polyhedral shapes obtained via the MCFSS analysis are given in Table II.

### B. MCRG analysis

The MCRG approach has been broadly used to estimate various critical exponents and percolation thresholds for continuum percolation of overlapping objects and hard-core-soft-shell models [3,32]. Herein, we follow the renormalization procedure described in Ref. [32], where Lee and Torquato [32] restricted themselves to one-parameter cell-to-cell transformation. A rescaling is implemented in which a cubic cell of size  $L$  is mapped onto a cell of size  $L_0$ . The recursion relation of the one-parameter cell-to-cell transformation can be written

as

$$P_0(\phi_0, L_0) = P(\phi, L) \quad (4)$$

where  $P_0$  is the percolation probability under the given  $\phi_0$  and  $L_0$ .  $P(\phi, L)$  corresponds to the  $P$ - $\phi$  curves for various  $L$  shown in Fig. 3.

Following Reynolds *et al.* [40] and Lee and Torquato [32], one can probe extrapolations of the correlation-length exponent  $\nu$  to the  $L/L_0 \rightarrow 0$  limit where the renormalization should be exact:

$$\ln(E_{L,L_0}) = k \ln(L/L_0) + c \quad (5)$$

where  $k = 1/\nu$  and  $c$  is a constant.  $E_{L,L_0}$  is the eigenvalue of the linearized transformation defined as

$$E_{L,L_0} = \left[ \frac{dP(\phi, L)}{d\phi} \right] \bigg/ \left[ \frac{dP(\phi, L_0)}{d\phi} \right] \bigg|_{\phi=\phi_{L,L_0}^*} \quad (6)$$

where  $\phi_{L,L_0}^*$  is the intersection value between  $P(\phi, L)$  and  $P(\phi, L_0)$  that approximates the critical value at which the percolating cluster just emerges at a finite-size system. According to Eqs. (5) and (6), once  $P(\phi, L)$ ,  $P(\phi, L_0)$ , and  $\phi_{L,L_0}^*$

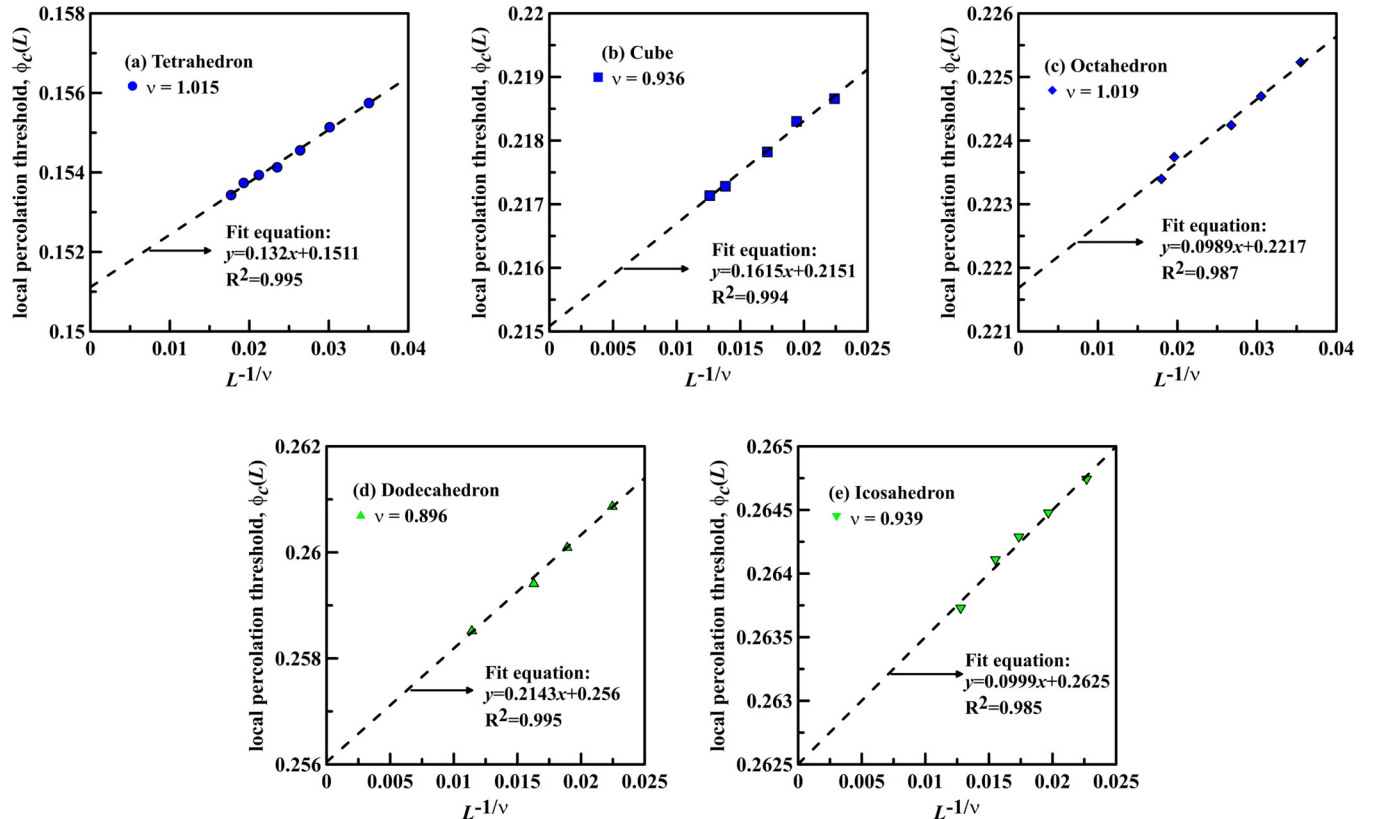


FIG. 6. The local percolation threshold  $\phi_c(L)$  vs  $L^{-1/\nu}$  for different polyhedral shapes: (a) tetrahedron, (b) cube, (c) octahedron, (d) dodecahedron, and (e) icosahedron. The symbols are the numerical results and the dashed lines are linear fittings.

TABLE II. Global percolation threshold  $\phi_c$  for the five polyhedral shapes obtained via the MCFSS analysis and the MCRG method. The derived numerical values are compared against the theoretical bounds. The superscript (\*) stands for  $\phi_c$  via  $\nu$  from MCRG ( $L_0 = 8$ ) in Table I.

$\phi_c$	Tetrahedron	Cube	Octahedron	Dodecahedron	Icosahedron
MCFSS	$0.1511 \pm 0.0012$	$0.2151 \pm 0.0012$	$0.2217 \pm 0.0014$	$0.2560 \pm 0.0008$	$0.2625 \pm 0.0010$
MCRG*	$0.1525 \pm 0.0012$	$0.2176 \pm 0.0014$	$0.2247 \pm 0.0010$	$0.2580 \pm 0.0005$	$0.2650 \pm 0.0008$
MCRG ( $\nu = 0.88$ )	$0.1516 \pm 0.0012$	$0.2169 \pm 0.0014$	$0.2231 \pm 0.0010$	$0.2578 \pm 0.0005$	$0.2640 \pm 0.0008$
Lower bound	0.0628	0.087	0.0898	0.1038	0.1061
Upper bound	0.1625	0.2202	0.2268	0.2590	0.2642

are determined, the correlation-length exponent  $\nu$  can thus be obtained from the reciprocal of the slope of a plot of  $\ln(E_{L,L_0})$  versus  $\ln(L/L_0)$ .

Additionally, as the cell size increases,  $P(\phi, L)$  approaches a step function (see Fig. 7) and a jump discontinuity occurs at  $\phi_{L,L_0}^* = f_c$ . The scaling relation from  $\phi_{L,L_0}^*$  to  $\phi_c$  is presented by

$$|\phi_{L,L_0}^* - \phi_c| \propto (L/L_0)^{-1/\nu}. \quad (7)$$

Consequently, once  $\phi_{L,L_0}^*$  and  $\nu$  are obtained, the global percolation threshold  $\phi_c$  can be determined from a plot of  $(L/L_0)^{-1/\nu}$  versus  $\phi_{L,L_0}^*$ , of which the value corresponds to the intercept on the abscissa of a plot of  $(L/L_0)^{-1/\nu}$  versus  $\phi_{L,L_0}^*$ .

In order to implement MCRG transformations introduced above, we additionally generate  $P$ - $\phi$  curves for selected transformation cells of  $L_0 = 8$  and 9 with the consideration of tetrahedral and cubic particle systems and the  $P$ - $\phi$  curves for  $L_0 = 8$  with the consideration of octahedral, dodecahedral, and icosahedral particle systems, using the Monte Carlo simulations described in Sec. II. Note that, for each polyhedral shape, we generate 800 000 realizations of  $L_0 = 8$  and 500 000 realizations of  $L_0 = 9$ . Combining with the systems of  $L = 30, 35, 40, 45, 50, 55$ , and 60 for the five polyhedral particle shapes presented in Sec. II, Fig. 7 plots the numerical data of  $P(\phi, L_0)$  and  $P(\phi, L)$  for the five polyhedral shapes and fitted results using Eq. (3).

Rescaling is performed for cells of  $L = 30, 35, 40, 45, 50, 55$ , and 60 onto the cells of  $L_0 = 8$  and 9. Thus, we can obtain

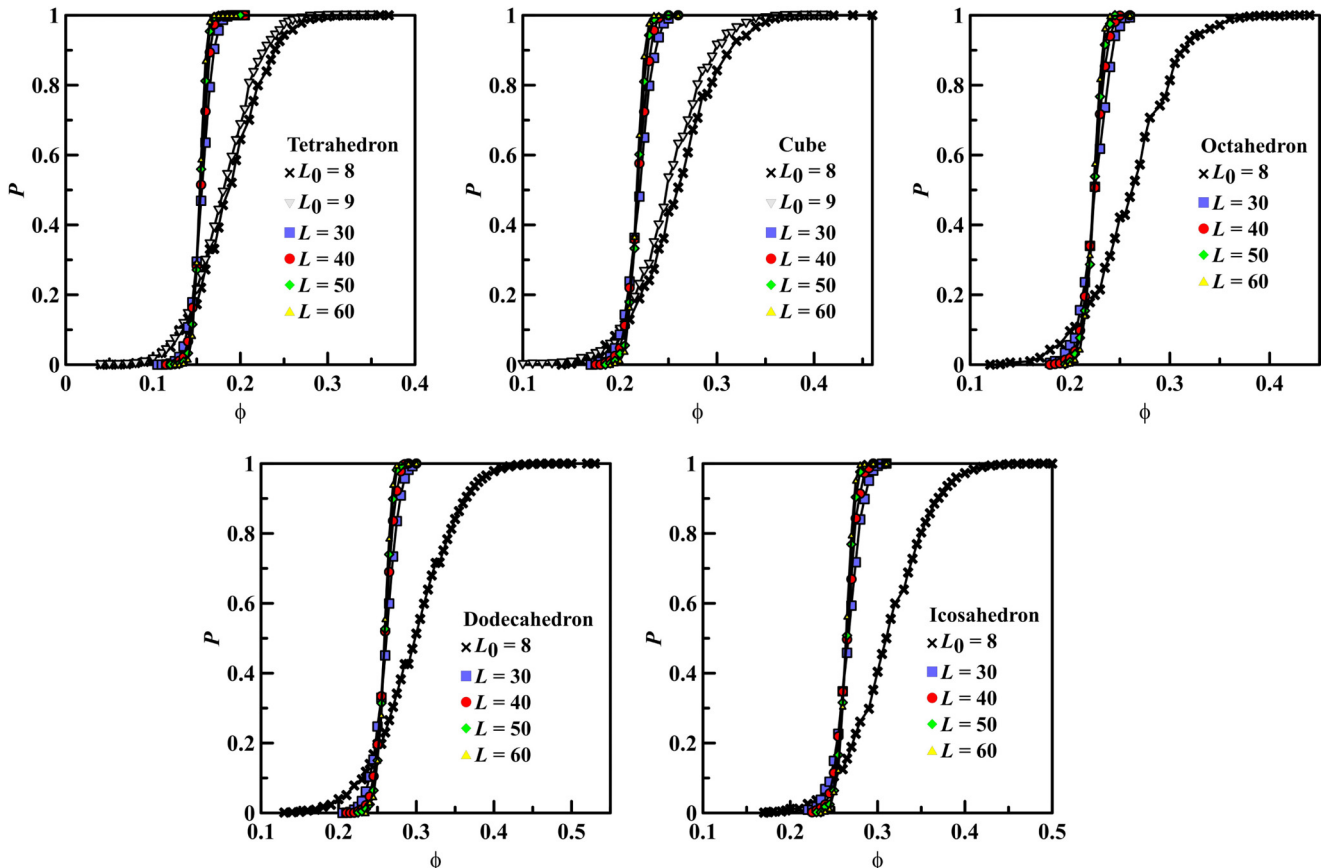


FIG. 7. The  $P$ - $\phi$  curves of different system sizes  $L_0$  and  $L$  for the five polyhedral shapes. The symbols are the numerical results and the lines are fittings.

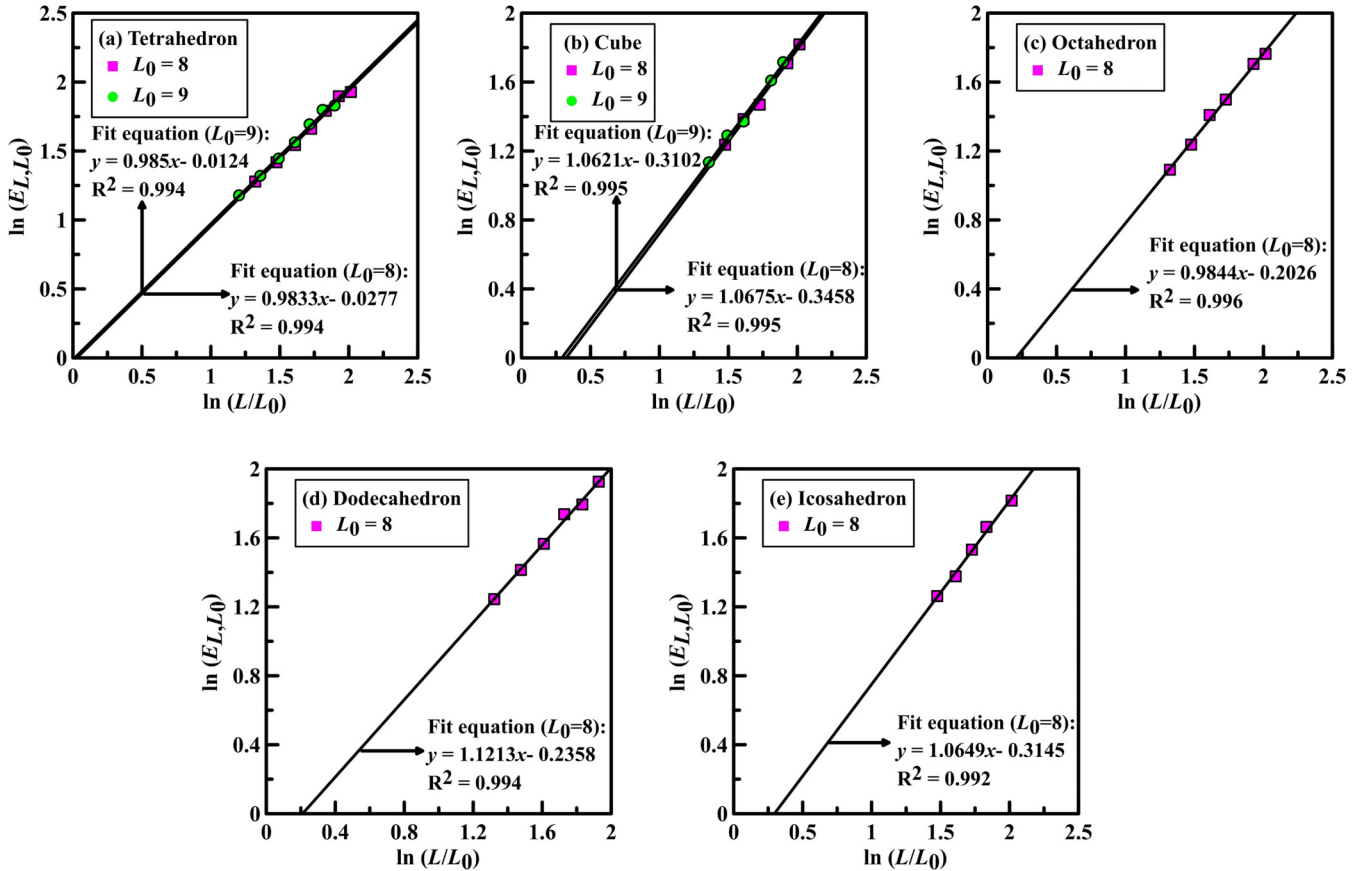


FIG. 8. The plots of  $\ln(E_{L,L_0})$  vs  $\ln(L/L_0)$  for the five polyhedral shapes. The correlation-length exponents  $\nu$  are the reciprocals of slopes of the linear fitting formulas shown in these figures.

the intersection values  $\phi_{L,L_0}^*$  between  $P(\phi, L)$  and  $P(\phi, L_0)$ , and even determine the eigenvalues  $E_{L,L_0}$  according to Eq. (6). We plot  $\ln(E_{L,L_0})$  versus  $\ln(L/L_0)$  for the five polyhedral shapes to determine the correlation-length exponents  $\nu$ , as shown in Fig. 8. From Figs. 8(a) and 8(b), one can clearly see that, for  $L_0 = 8$  and 9, the corresponding slopes and  $R^2$  of the linear fittings are well consistent. This is why we select the single  $L_0 = 8$  as the subsequent transformation for the octahedral, dodecahedral, and icosahedral shapes. Table I displays  $\nu$  for the five polyhedral shapes using the present MCRG approach and gives the comparison against that from MCFSS analysis. Moreover, we utilize the MCRG analysis [see Eq. (7)] to estimate the global percolation thresholds  $\phi_c$  for the five polyhedral shapes from the plots of  $(L/L_0)^{-1/\nu}$  versus  $\phi_{L,L_0}^*$ , as shown in Fig. 9; since  $L/L_0$  tends to infinite, the intersection values  $\phi_{L,L_0}^*$  for  $L_0 = 8$  and 9 are expected to approach a single value  $\phi_c$ , as shown in Figs. 9(a) and 9(b). As such, for the subsequent octahedral, dodecahedral, and icosahedral shapes, we just utilize  $L_0 = 8$  as a rescaling to map onto cells of various  $L$ . The global percolation thresholds for the five polyhedral shapes are estimated from the intercepts on the abscissa in the plots and compared against the percolation thresholds derived from the same  $L_0$  and  $\nu = 0.88$ , as shown in Figs. 9(c)–9(g). From these figures, one can find that, for each polyhedral shape,  $R^2$  values of the linear fittings from both values of  $\nu$  (one is our numerical value and another is  $\nu = 0.88$ ) are the same. Also, the estimated global percolation

thresholds of  $\phi_c$  from both options are very close though  $\phi_c$  via  $\nu$  from our numerical analysis is somewhat larger than that via  $\nu = 0.88$ . The reason is that our numerical value of  $\nu$  is slightly larger than the known value of  $\nu = 0.88$ , which causes the value of  $(L/L_0)^{-1/\nu}$  via  $\nu$  from our numerical analysis to be larger than that of  $(L/L_0)^{-1/\nu}$  via  $\nu = 0.88$ , under the same other conditions. The detailed values of the global percolation threshold from both options are tabulated in Table II.

### C. Correlation-length exponent $\nu$

Table I presents the correlation-length exponents  $\nu$  for the five polyhedral shapes using the MCFSS analysis [on the basis of Fig. 5(b)] and the MCRG approach (on the basis of Fig. 8). We clearly see that the two scaling methods can generate similar results of  $\nu$  for a single polyhedral shape. For different polyhedral shapes, the statistical values of  $\nu$  are close, which seems to confirm the universality of the correlation-length exponent in continuum percolation of overlapping polyhedral particles, but appear to be slightly larger than the value of  $\nu = 0.88$  in lattice percolation, as shown in Table I. Such discrepancies are mainly attributed to the following three aspects.

(1) The present controllable parameter is the volume fraction  $\phi$  of overlapping particles. Nevertheless, as noted by Lee and Torquato [32], a formulation in terms of  $\phi$  has a drawback in that  $\phi$  is not a controllable simulation parameter

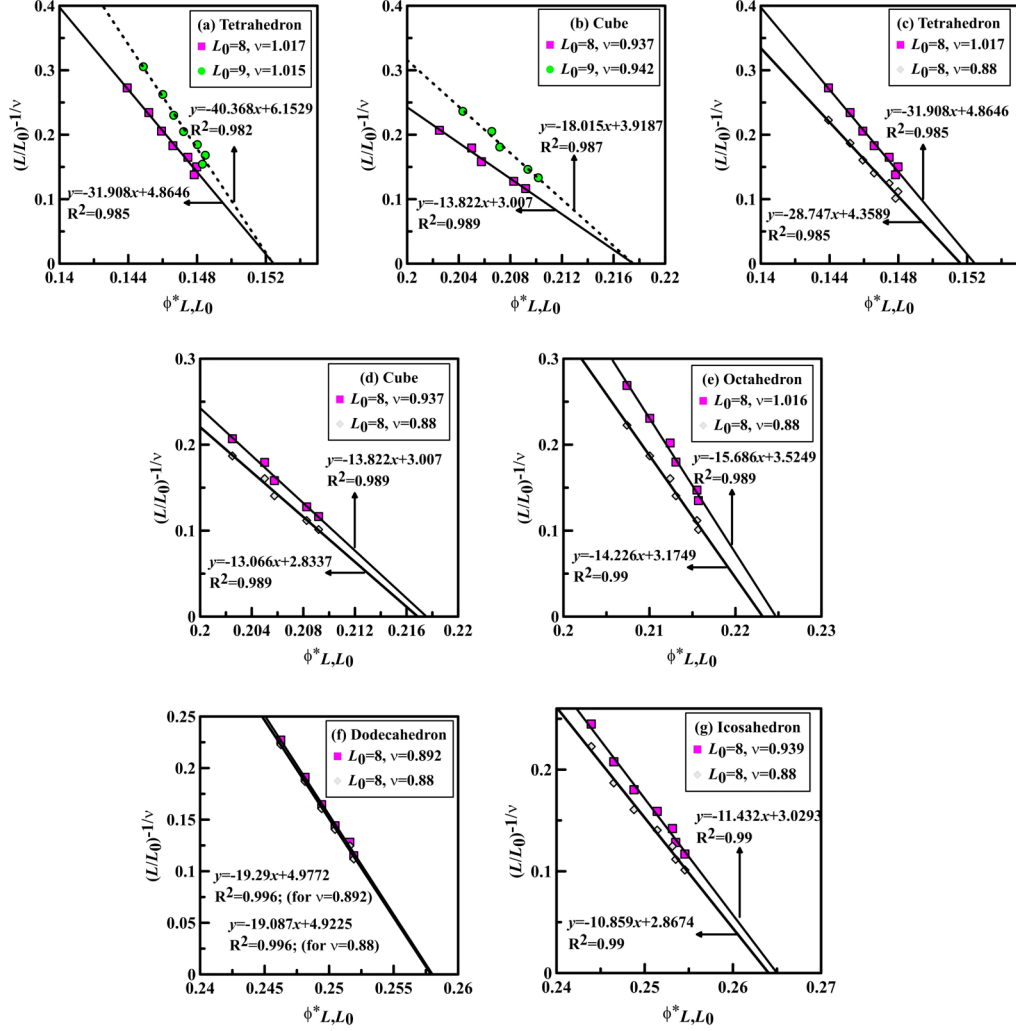


FIG. 9. The plots of  $(L/L_0)^{-1/\nu}$  vs  $\phi^*_{L,L_0}$  for the five polyhedral shapes.

in continuum percolation.  $\phi$  for any finite-size system varies from realization to realization for a given reduced number density  $\eta$  because of different overlapping degrees among the particles.

(2) The present input parameter is the volume fraction  $\phi$  of overlapping particles, and then  $\phi$  is converted into the number of particles using Eq. (1) in the present Monte Carlo simulations. However, on the one hand, Eq. (1) is just an approximation for finite-size systems that is exact for an infinite-size system; on the other hand, the round-up values from Eq. (1) have to be used to meet the integer of the number of particles.

(3) The selected maximum size of present realizations is  $L = 60$  that may not meet the requirement of accurately estimating the correlation-length exponent. As mentioned in the book of Stauffer and Aharony [3], the determination of the correlation-length exponent needs far more and larger realizations than the determination of the percolation threshold.

#### D. Global percolation threshold $\phi_c$

Table II presents the global percolation thresholds  $\phi_c$  for the five polyhedral shapes obtained via the MCFSS analysis

(on the basis of Fig. 6) and the MCRG approach (on the basis of Fig. 9). In the MCRG approach, we prescribe two cases of  $\nu$ , one from our numerical simulations (see the third line in Table I) and another that is the universal value of  $\nu = 0.88$  in lattice percolation, to estimate the percolation thresholds of the five polyhedral shapes for purpose of comparison. In addition, our numerical results of  $\phi_c$  are further compared against the theoretical bounds, as shown in Table II. Similar to  $\Delta$  shown in Fig. 5, we can see that  $\phi_c$  increases in the following order: tetrahedron < cube < octahedron < dodecahedron < icosahedron. We therefore conclude that  $\phi_c$  and  $\Delta$  increase with increasing number of faces at least for the five polyhedral shapes. This also indicates that polyhedral particles that are closer to spheres (i.e., more “spherical”) are more difficult to percolate than those that are far from spherical shapes. This trend seems to be in agreement with that for systems containing ellipsoidal and spherocylindrical particles reported in the literature [16–22]. In addition, Table II shows that all numerical results of  $\phi_c$  from the MCFSS analysis and the MCRG approach are well within the theoretical excluded-volume bounds, although they tend to be closer to the upper bound. It further reveals that the two numerical frameworks can accurately estimate the global percolation threshold  $\phi_c$

TABLE III. Global percolation threshold characterized by the critical reduced number density  $\eta_c$  for the five polyhedral shapes via the two approaches presented in Table II.

$\eta_c$	Tetrahedron	Cube	Octahedron	Dodecahedron	Icosahedron
MCFSS	0.1638	0.2422	0.2505	0.2964	0.3041
MCRG*	0.1655	0.2454	0.2545	0.2984	0.3079
MCRG ( $\nu = 0.88$ )	0.1644	0.2445	0.2524	0.2981	0.3065
Ref. [15]	$0.1701 \pm 0.0007$	$0.2443 \pm 0.0005$	$0.2514 \pm 0.0006$	$0.2949 \pm 0.0005$	$0.3030 \pm 0.0005$

for polyhedral particles. The theoretical bounds are introduced as follows. Moreover, for a single polyhedral shape, Table II shows that  $\phi_c$  from the MCRG\* method is greater than  $\phi_c$  from the MCRG ( $\nu = 0.88$ ) approach, which is greater than  $\phi_c$  from the MCFSS analysis. Note that the error bars shown in Tables I and II are calculated in terms of the standard error form. We select six groups of SN = 2500, 5000, 7500, 10 000, 12 500, and 15 000, where SN is the number of samples. On the basis of the percolation probabilities  $P(\phi, L)$  of each group, we calculate the correlation-length exponent and percolation threshold of each group in terms of the MCFSS analysis and the MCRG method described in this paper. Essentially, we need to repeat six times the present MCFSS analysis and the MCRG method for each polyhedral shape. Then, according to the six statistical values of  $\nu$  and  $\phi_c$  for each polyhedral shape, we invoke the standard error function in MATLAB software to compute the individual standard errors.

It is worth mentioning that the percolation threshold is sometimes characterized by the critical reduced number density  $\eta_c$ . The reduced number density of overlapping particles is related to the volume fraction:  $\phi = 1 - e^{-\nu}$ . Note that, as mentioned above, the relation is exact only for an infinite-size system. Table III presents the numerical results of  $\eta_c$  for the five polyhedral shapes via the two approaches presented in Table II and a comparison with the corresponding numerical values reported by Torquato and Jiao [15]. We find that the present numerical results of  $\eta_c$  generally agree with the corresponding numerical values reported in Ref. [15]. Moreover, the dependency of  $\eta_c$  on the five polyhedral shapes is fully consistent with that of  $\phi_c$  and  $\Delta$ . However, we note that the  $\eta_c$  values obtained in this paper are slightly different from the corresponding ones reported in Ref. [15]. These small discrepancies might be caused by the different methods employed for obtaining  $\eta_c$ : in this paper, the MCFSS analysis and the MCRG method are used, while in Ref. [15] the percolation thresholds of finite systems with various system sizes were extrapolated to estimate the infinite system limits.

Equations (8) and (9) present the bounds for the percolation threshold of overlapping polyhedral particles. Equation (8)

describes the excluded-volume percolation model for an arbitrary convex object system [15,22], i.e.,

$$\phi_c = \begin{cases} 1 - e^{-1/V_{d,ex}} & \text{the lower bound} \\ 1 - e^{-2.7344/V_{d,ex}} & \text{the upper bound} \end{cases} \quad (8)$$

where  $V_{d,ex}$  is the dimensionless excluded volume of the particle, namely,  $V_{d,ex} = V_{ex}/V$ , where  $V_{ex}$  is the excluded volume that is defined as a volume in which two particle centers must be in order for the particles to overlap. The excluded volume of polyhedral particles can be determined theoretically and numerically by the second virial coefficient and Monte Carlo simulations [34,41]. Herein, we directly present the analytical expression of  $V_{d,ex}$  for the five polyhedral shapes, as given in Eq. (9):

$$V_{d,ex} = \frac{3Eb}{\pi s} \arccos\left(\frac{\cos(\pi/f)}{\sin(\pi/n)}\right) + 2 \quad (9)$$

where  $f$  and  $n$  are the number of faces connected by each vertex and the number of sides of each face, respectively.  $E$  is the number of sides of a polyhedron.  $s$  is sphericity defined as the ratio between the surface area of a sphere and that of a polyhedron with the same volume [34,41]. For a regular tetrahedron,  $s = 0.671$ ,  $f = n = 3$ , and  $E = 6$ . For a cube,  $s = 0.806$ ,  $f = 3$ ,  $\nu = 4$ , and  $E = 12$ . For a regular octahedron,  $s = 0.846$ ,  $f = 4$ ,  $\nu = 3$ , and  $E = 12$ . For a regular dodecahedron,  $s = 0.91$ ,  $f = 3$ ,  $n = 5$ , and  $E = 30$ . For a regular icosahedron,  $s = 0.939$ ,  $f = 5$ ,  $n = 3$ , and  $E = 30$ . We note that Eq. (9) is validated by the comparison of numerical results from the Monte Carlo simulations reported by Xu *et al.* [34], as shown in Table IV.

#### IV. CONCLUSIONS AND DISCUSSION

We have presented two numerical frameworks, the MCFSS analysis and the MCRG method, to systematically study the continuum percolation of randomly oriented overlapping polyhedral particles, which have been shown to be sound approaches for deriving the percolation properties. The proposed numerical frameworks suggest the generic procedures for the study of continuum percolation of nonspherical

TABLE IV. Dimensionless excluded volumes  $V_{d,ex}$  for the five polyhedral shapes derived by Eq. (9) and the Monte Carlo simulations.

$V_{d,ex}$	Tetrahedron	Cube	Octahedron	Dodecahedron	Icosahedron
Theory	15.41	10.99	10.63	9.12	8.91
Simulation	15.39	10.93	10.64	9.03	8.79

particles. Additionally, the excluded-volume percolation bounds for different polyhedral shapes are consistent with the numerical results obtained via our frameworks. The obtained results reveal that the percolation threshold characterized by the critical volume fraction  $\phi_c$  or the critical reduced number density  $\eta_c$  and the percolation transition width  $\Delta$  are monotonic increasing functions of the number of polyhedral faces. Our results of  $\phi_c$  and the theoretical bounds can guide the evaluation of the structure-property relation of nonspherical particle systems. The ideas presented here can be extended by applying them in the evaluation of the effect of  $\phi_c$  on the structural, transport, and

mechanical properties of porous materials composed of nonspherical particles.

### ACKNOWLEDGMENTS

This work was supported by the National Natural Science Foundation of China (Grants No. 11772120, No. 11802084, and No. 11402076), the Natural Science Foundation of Jiangsu Province (Grant No. BK20170096), and the Fundamental Research Funds for the Central Universities (Grant No. 2016B06314). The State Scholarship Fund from China Scholarship Council is greatly acknowledged.

- 
- [1] S. Torquato, *Random Heterogeneous Materials: Microstructure and Macroscopic Properties* (Springer-Verlag, New York, 2002).
  - [2] M. Sahimi, *Heterogeneous Materials I: Linear Transport and Optical Properties* (Springer-Verlag, Berlin, 2003).
  - [3] D. Stauffer and A. Aharony, *Introduction to Percolation Theory*, 2nd rev. ed. (Taylor & Francis, London, 2003).
  - [4] A. G. Hunt, *Percolation Theory for Flow in Porous Media*, Lecture Notes in Physics (Springer-Verlag, Berlin, 2005).
  - [5] I. Balberg, *Phys. Rev. B* **31**, 4053 (1985); **33**, 3618 (1986); *Phys. Rev. Lett.* **59**, 1305 (1987).
  - [6] V. V. Mourzenko, J.-F. Thovert, and P. M. Adler, *Phys. Rev. E* **84**, 036307 (2011).
  - [7] W. X. Xu, D. Zhang, P. Lan, and Y. Jiao, *Int. J. Mech. Sci.* **150**, 610 (2019).
  - [8] W. X. Xu, Y. Wu, and M. Jia, *Compos. Struct.* **203**, 124 (2018).
  - [9] W. X. Xu, M. Jia, and Z. Gong, *Compos. Sci. Technol.* **167**, 134 (2018).
  - [10] W. X. Xu, Z. Zhu, and D. Zhang, *Soft Matter* **14**, 8684 (2018).
  - [11] W. X. Xu, F. Wu, Y. Jiao, and M. Liu, *Mater. Design* **127**, 162 (2017).
  - [12] M. D. Rintoul and S. Torquato, *J. Phys. A: Math. Gen.* **30**, L585 (1997).
  - [13] G. Lois, J. Blawdziewicz, and C. S. O'Hern, *Phys. Rev. Lett.* **102**, 015702 (2009).
  - [14] R. M. Ziff and S. Torquato, *J. Phys. A: Math. Theoret.* **50**, 085001 (2017).
  - [15] S. Torquato and Y. Jiao, *J. Chem. Phys.* **137**, 074106 (2012); *Phys. Rev. E* **87**, 022111 (2013).
  - [16] E. J. Garboczi, K. A. Snyder, J. F. Douglas, and M. F. Thorpe, *Phys. Rev. E* **52**, 819 (1995).
  - [17] Y. B. Yi and A. M. Sastry, *Phys. Rev. E* **66**, 066130 (2002); *Proc. R. Soc. A* **460**, 2353 (2004).
  - [18] R. M. Mutiso, M. C. Sherrott, J. Li, and K. I. Winey, *Phys. Rev. B* **86**, 214306 (2012).
  - [19] H. Meyer, P. van der Schoot, and T. Schilling, *J. Chem. Phys.* **143**, 044901 (2015).
  - [20] B. Nigro, C. Grimaldi, P. Ryser, A. P. Chatterjee, and P. van der Schoot, *Phys. Rev. Lett.* **110**, 015701 (2013).
  - [21] A. P. Chatterjee, *J. Phys.: Condens. Matter* **20**, 255250 (2008); **27**, 375302 (2015).
  - [22] W. X. Xu, X. Su, and Y. Jiao, *Phys. Rev. E* **94**, 032122 (2016).
  - [23] W. X. Xu and Y. Jiao, *Int. J. Eng. Sci.* **134**, 31 (2019).
  - [24] M. O. Saar and M. Manga, *Phys. Rev. E* **65**, 056131 (2002).
  - [25] M. Mathew, T. Schilling, and M. Oettel, *Phys. Rev. E* **85**, 061407 (2012).
  - [26] J. Lin, H. Chen, and W. X. Xu, *Phys. Rev. E* **98**, 012134 (2018).
  - [27] S. Torquato and Y. Jiao, *Nature (London)* **460**, 876 (2009).
  - [28] R. Xiao and C. Tian, *J. Mech. Phys. Solids* **125**, 472 (2019).
  - [29] H. Malmir, M. Sahimi, and M. R. Rahimi Tabar, *Sci. Rep.* **6**, 35024 (2016); *Phys. Rev. E* **94**, 062901 (2016).
  - [30] U. Alon, A. Drory, and I. Balberg, *Phys. Rev. A* **42**, 4634 (1990).
  - [31] D. R. Baker, G. Paul, S. Sreenivasan, and H. E. Stanley, *Phys. Rev. E* **66**, 046136 (2002).
  - [32] S. B. Lee and S. Torquato, *Phys. Rev. A* **41**, 5338 (1990).
  - [33] W. X. Xu, Z. Han, L. Tao, Q. Ding, and H. Ma, *Powder Technol.* **323**, 301 (2018).
  - [34] W. X. Xu, G. Yang, P. Lan, and H. Ma, *Comput. Mater. Con.* **52**, 25 (2016).
  - [35] X. Xu, J. F. Wang, J. P. Lv, and Y. J. Deng, *Front. Phys.* **9**, 113 (2014).
  - [36] M. E. J. Newman and R. M. Ziff, *Phys. Rev. Lett.* **85**, 4104 (2000);
  - [37] A. Coniglio, *J. Phys. A* **15**, 3829 (1982).
  - [38] T. Kalisky and R. Cohen, *Phys. Rev. E* **73**, 035101 (2006).
  - [39] C. D. Lorenz and R. M. Ziff, *J. Chem. Phys.* **114**, 3659 (2001).
  - [40] P. J. Reynolds, H. E. Stanley, and W. Klein, *Phys. Rev. B* **21**, 1223 (1980).
  - [41] W. X. Xu, H. Sun, W. Chen, and H. Chen, *Int. J. Mod. Phys. B* **32**, 1840011 (2018).